

# Thickness-scaling phonon resonance: A systematic study of hexagonal boron nitride from monolayers to bulk crystals <sup>EP</sup>

Cite as: J. Appl. Phys. **132**, 134302 (2022); <https://doi.org/10.1063/5.0094039>

Submitted: 11 August 2022 • Accepted: 07 September 2022 • Published Online: 03 October 2022

Xiaojie Jiang, Mingyuan Chen,  Jiahan Li, et al.

## COLLECTIONS

 This paper was selected as an Editor's Pick



View Online



Export Citation



CrossMark

## ARTICLES YOU MAY BE INTERESTED IN

[Quasi-periodic Andreev reflection in topological nodal-line semimetal-superconductor junctions](#)

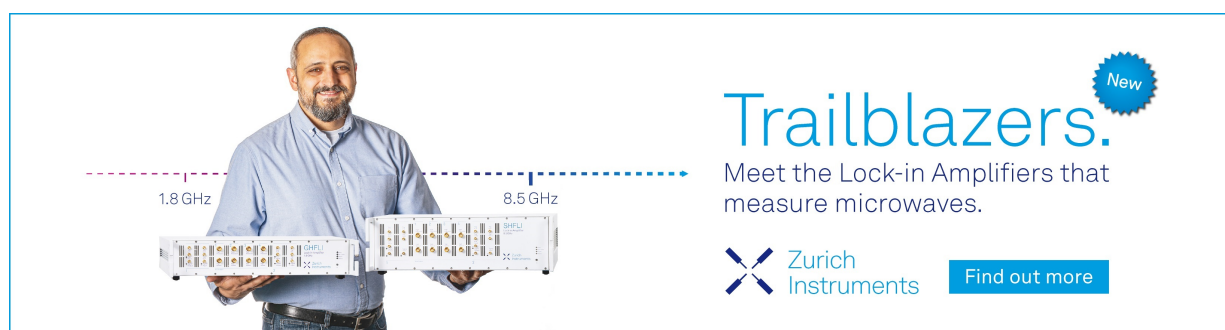
Journal of Applied Physics **132**, 134303 (2022); <https://doi.org/10.1063/5.0102989>

[The effects of Tb doping on the negative and positive magnetocaloric effects of  \$Mn\_3Ga\_{1-x}Tb\_xC\$  \( \$0.02 \leq x \leq 0.05\$ \)](#)

Journal of Applied Physics **132**, 135108 (2022); <https://doi.org/10.1063/5.0111987>

[Terahertz topological photonic integrated circuits for 6G and beyond: A Perspective](#)

Journal of Applied Physics **132**, 140901 (2022); <https://doi.org/10.1063/5.0099423>



**Trailblazers.** <sup>New</sup>

Meet the Lock-in Amplifiers that measure microwaves.

Zurich Instruments [Find out more](#)

# Thickness-scaling phonon resonance: A systematic study of hexagonal boron nitride from monolayers to bulk crystals

Cite as: J. Appl. Phys. **132**, 134302 (2022); doi: [10.1063/5.0094039](https://doi.org/10.1063/5.0094039)

Submitted: 11 August 2022 · Accepted: 7 September 2022 ·

Published Online: 3 October 2022



View Online



Export Citation



CrossMark

Xiaojie Jiang,<sup>1,2</sup> Mingyuan Chen,<sup>1</sup> Jiahao Li,<sup>3</sup>  Parvin Fathi-Hafshejani,<sup>4</sup> Jialiang Shen,<sup>1</sup> Yiming Jin,<sup>2</sup> Wei Cai,<sup>2,5,a)</sup>  Masoud Mahjouri-Samani,<sup>4</sup>  James H. Edgar,<sup>3</sup> and Siyuan Dai<sup>1,a)</sup> 

## AFFILIATIONS

<sup>1</sup>Department of Mechanical Engineering, Materials Research and Education Center, Auburn University, Auburn, Alabama 36849, USA

<sup>2</sup>The Key Laboratory of Weak-Light Nonlinear Photonics, Ministry of Education, School of Physics and TEDA Applied Physics Institute, Nankai University, Tianjin 300457, People's Republic of China

<sup>3</sup>Tim Taylor Department of Chemical Engineering, Kansas State University, Manhattan, Kansas 66506, USA

<sup>4</sup>Department of Electrical and Computer Engineering, Auburn University, Auburn, Alabama 36849, USA

<sup>5</sup>Collaborative Innovation Center of Extreme Optics, Shanxi University, Taiyuan, Shanxi 030006, People's Republic of China

<sup>a)</sup>Authors to whom correspondence should be addressed: [sdai@auburn.edu](mailto:sdai@auburn.edu) and [weicai@nankai.edu.cn](mailto:weicai@nankai.edu.cn)

## ABSTRACT

Phonons are important lattice vibrations that affect the thermal, electronic, and optical properties of materials. In this work, we studied infrared phonon resonance in a prototype van der Waals (vdW) material—hexagonal boron nitride (hBN)—with the thickness ranging from monolayers to bulk, especially on ultra-thin crystals with atomic layers smaller than 20. Our combined experimental and modeling results show a systematic increase in the intensity of in-plane phonon resonance at the increasing number of layers in hBN, with a sensitivity down to one atomic layer. While the thickness-dependence of the phonon resonance reveals the antenna nature of our nanoscope, the linear thickness-scaling of the phonon polariton wavelength indicates the preservation of electromagnetic hyperbolicity in ultra-thin hBN layers. Our conclusions should be generic for fundamental resonances in vdW materials and heterostructures where the number of constituent layers can be conveniently controlled. The thickness-dependent phonon resonance and phonon polaritons revealed in our work also suggest vdW engineering opportunities for desired thermal and nanophotonic functionalities.

Published under an exclusive license by AIP Publishing. <https://doi.org/10.1063/5.0094039>

## I. INTRODUCTION

Lattice vibrations referred to as phonons play an important role in a wealth of material properties: they affect thermal conductivity,<sup>1,2</sup> electron mobility,<sup>3,4</sup> and light–matter interactions.<sup>5</sup> The proper control and utilization of phonons have led to a series of advances, including radiative cooling,<sup>6</sup> heat transfer manipulation,<sup>7,8</sup> and mechanical sensing.<sup>9</sup> In polar materials, phonons can couple with photons to form hybridized light–matter modes called phonon polaritons.<sup>10</sup> They exist inside the Reststrahlen band, where the frequency  $\omega$  is between the transverse and longitudinal optical modes ( $\omega_{TO} < \omega < \omega_{LO}$ ). Phonon polaritons can be described as “nanoscale light propagating in materials”: they propagate as

electromagnetic waves, depend on material properties, and are highly confined—with a wavelength ( $\lambda_p$ ) much smaller than that of photons in free space ( $\lambda_0$ ). Therefore, phonon polaritons offer an opportunity to investigate optics and light–matter interactions at small scales<sup>11,12</sup> and lead to valuable applications, such as super-resolution imaging<sup>13</sup> and phonon polaritonic molecular sensing.<sup>14</sup> Recently, anisotropic phonon polaritons were reported in van der Waals (vdW) materials of hexagonal boron nitride (hBN)<sup>15–22,24</sup> and  $\alpha$ -phase molybdenum trioxide ( $\alpha$ -MoO<sub>3</sub>).<sup>25–27,29,30</sup> Their natural hyperbolicity<sup>29,30</sup> (permittivity  $\epsilon_i \epsilon_j < 0$ ,  $i$  and  $j$  as  $x$ ,  $y$ , or  $z$ ) is useful for the extreme control of light at a length scale down to the interatomic spacing and with low dissipation. Phonon

polaritons have been observed in hBN with a thickness down to monolayer,<sup>31</sup> and a scaling law has been reported for hBN with the thickness spanning from 20 to 1500 layers.<sup>17</sup> The advantages of vdW materials originate from their layered nature, where the crystal thickness can be delicately controlled via the layer number  $N$ . Physical properties of vdW materials typically evolve with the layer number  $N$ , especially at the reduced dimension with the thickness of few atomic layers. However, the detailed evolution of phonon resonances in hBN with  $N$ , from monolayer to bulk crystals, remains unexplored.

In this work, we report a combined experimental and theoretical study of the scaling of infrared (IR) phonon resonance and phonon polaritons with the thickness from monolayer to hundreds of layers in both naturally abundant hBN and isotopically pure  $h^{10}\text{BN}$  and  $h^{11}\text{BN}$ <sup>32,33</sup> crystals. Our focus on crystals with  $N < 20$  reveals dissimilar thickness-dependences for phonon resonance and phonon polaritons. While the intensity of the phonon resonance increases with  $N$ , the thickness-dependence seems to be affected by the technical nature of the antenna-based nano-IR microscopy in our experiments. In contrast, the phonon polaritons' wavelength  $\lambda_p$  scales linearly with  $N < 20$ . These thickness-dependences reported in our work will offer guidance to control phonon resonances and phonon polaritons by engineering vdW layers for desired thermal and nanophotonic functionalities.

## II. THICKNESS-SCALING OF PHONON RESONANCE

The naturally abundant hBN (contains  $\sim 80\%$   $^{11}\text{B}$  and  $\sim 20\%$   $^{10}\text{B}$ ) and isotopically pure  $h^{10}\text{BN}$  (99.22%  $^{10}\text{B}$ ) and  $h^{11}\text{BN}$  (99.41%  $^{11}\text{B}$ ) crystals were mechanically exfoliated onto a Si substrate with a 285 nm thick  $\text{SiO}_2$  layer on top. The study of IR phonon resonance

and phonon polaritons was performed using scattering-type scanning near-field optical microscopy (s-SNOM, [supplementary material](#)). The s-SNOM [Fig. 1(a)] is based on a tapping-mode atomic force microscope (AFM) that simultaneously delivers topography (3D structure) and optical image (false color) of the scanned sample with a resolution close to the radius of the AFM tip ( $a \sim 20$  nm). In the experiment, a continuous-wave IR laser (solid green arrow) is focused on the apex of a metalized AFM tip, which acts as an optical antenna generating a strong optical near-field. This strong near-field interacts with the sample, gets back-scattered off the tip (dashed green arrow), and is detected as experimental observables s-SNOM amplitude  $S(\omega)$  and phase  $\Phi(\omega)$  related to the local optical response of the sample underneath the AFM tip. For polaritonic materials, the generated strong near-field can launch polaritons<sup>17</sup> that propagate to the edge of the sample and get reflected back to the tip. During the scan, polariton standing waves form via the interference between launched and reflected polaritons and can be visualized in the s-SNOM images.<sup>16,17</sup>

To study the thickness-scaling of phonon resonance, we performed the s-SNOM experiments at the transverse optical frequency  $\omega_{\text{TO}}$  of the in-plane phonon resonance in hBN. For naturally abundant hBN, representative s-SNOM amplitude images at  $\omega_{\text{TO}} = 1366 \text{ cm}^{-1}$  are plotted in Fig. 1. The  $\omega_{\text{TO}}$  was obtained from the Raman spectrum [Fig. 2(a), inset, also see [supplementary material](#) for details] of the exfoliated crystals. Combined AFM topography (3D structure) and s-SNOM image (false color) in Fig. 1(a) reveals distinct intensities of the phonon resonance via s-SNOM amplitude  $S(\omega)$  on hBN with the thickness of 2, 4, 6, 10, and 15 layers. Thicker crystals exhibit higher s-SNOM amplitude  $S(\omega)$  and correspond to higher intensity of the phonon resonance. Note that different from previous s-SNOM studies,<sup>16–22,31</sup> which

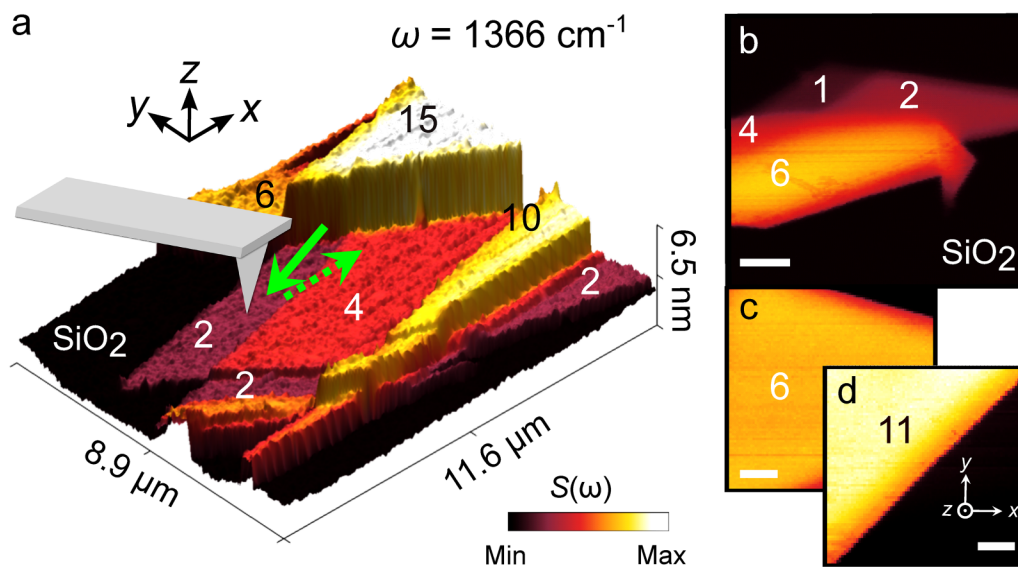


**FIG. 1.** Infrared nano-imaging on ultra-thin hBN. (a) The experiment schematic and combined topography (3D structure) and s-SNOM amplitude image [false color,  $S(\omega)$ ] of terraced hBN with the layer number  $N$  indicated in each area. (b)–(d) Representative s-SNOM amplitude images on the hBN monolayer and multilayers. Scale bar: 500 nm. IR frequency  $\omega = 1366 \text{ cm}^{-1}$ .

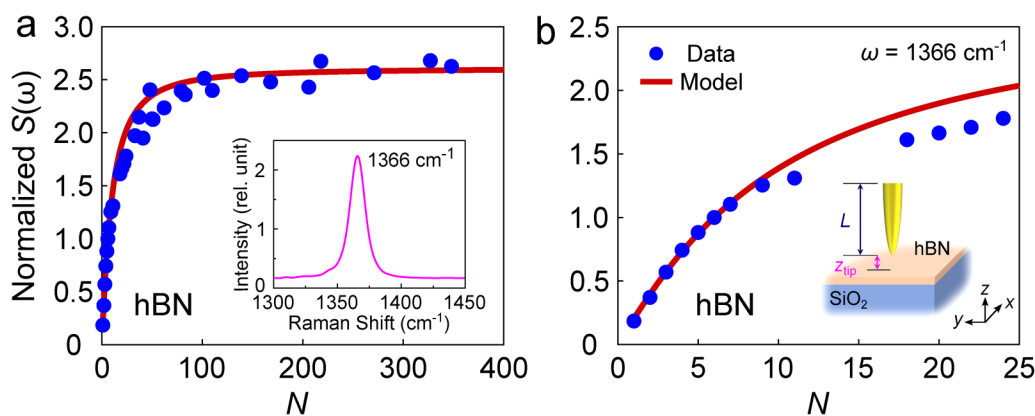


**FIG. 2.** The scaling of phonon resonance with the number of layers in naturally abundant hBN. (a) The s-SNOM amplitude  $S(\omega)$  (blue dots) measured from hBN with a variety of layer numbers  $N$ . Modeling results are plotted with the red curve. Inset, Raman spectrum of the naturally abundant hBN. (b) The zoom-in plot of (a) reveals the scaling of phonon resonance with the number of layers  $N$  in ultra-thin hBN ( $N < 20$ ). Inset, the schematic of the model for the s-SNOM experiment. IR frequency  $\omega = 1366 \text{ cm}^{-1}$ .

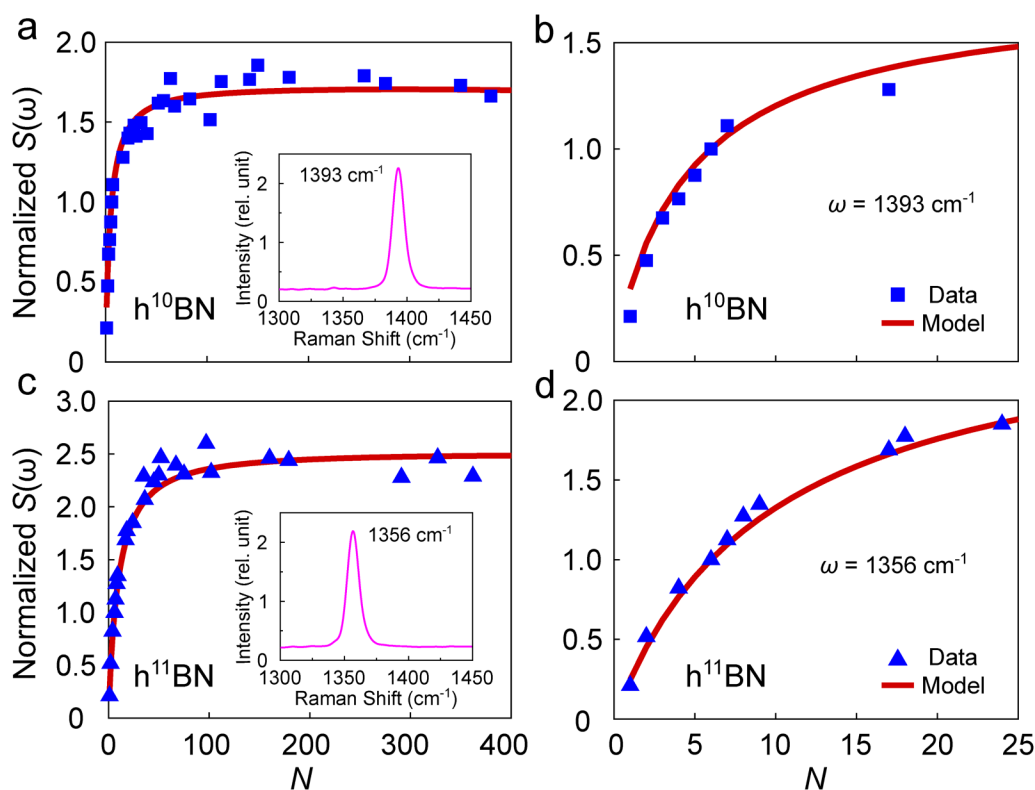


**FIG. 3.** The scaling of phonon resonance with the number of layers in isotopically pure  $h^{10}\text{BN}$  and  $h^{11}\text{BN}$ . (a) and (b) The s-SNOM amplitude  $S(\omega)$  (false color) was measured from  $h^{10}\text{BN}$  with a variety of layer numbers  $N$ . Modeling results are plotted with the red curve. Inset in (a), Raman spectrum of  $h^{10}\text{BN}$ . IR frequency in (a) and (b)  $\omega = 1393 \text{ cm}^{-1}$ . (c) and (d) The s-SNOM amplitude  $S(\omega)$  (false color) was measured from  $h^{11}\text{BN}$  with a variety of layer numbers  $N$ . Modeling results are plotted with the red curve. Inset in (a), Raman spectrum of  $h^{11}\text{BN}$ . IR frequency in (a) and (b)  $\omega = 1356 \text{ cm}^{-1}$ .

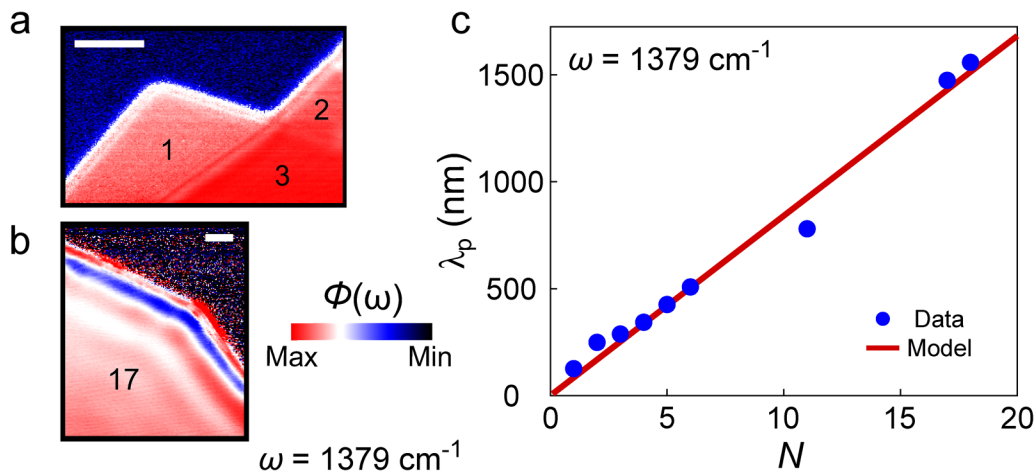


**FIG. 4.** The scaling of phonon polaritons with the number of layers in ultra-thin hBN ( $N < 20$ ). (a) and (b) Representative s-SNOM phase images  $\Phi(\omega)$  (false color) measured from the monolayer and multilayer hBN where the layer number  $N$  is marked in each area. IR frequency  $\omega = 1379 \text{ cm}^{-1}$ . Scale bar: 500 nm. (c) The scaling of the wavelength  $\lambda_p$  of phonon polaritons with the layer number  $N$  in ultra-thin hBN ( $N < 20$ ). Experimental data are indicated with blue dots, while the modeling results are plotted with the red curve.

focus on imaging hBN phonon polaritons inside the Reststrahlen band ( $\omega_{\text{TO}} < \omega < \omega_{\text{LO}}$ ), here we performed the s-SNOM imaging at the  $\omega_{\text{TO}}$  of hBN. Therefore, there are no evident phonon polariton fringes but only uniform s-SNOM signals related to intensities of the phonon resonance in hBN. We have conducted a systematic study of the phonon resonance in hBN of monolayers [Fig. 1(b)], few layers [Figs. 1(c) and 1(d)], and bulk crystals [Fig. 2(a)]. The dependence of the phonon resonance intensity with the layer number  $N$  is evidently revealed in our experiments [Figs. 1(b)–1(d)].

We summarize in Figs. 2(a)–2(b) the systematic evolution of the intensity of phonon resonance [as s-SNOM amplitude  $S(\omega)$ ] on hBN crystals with the layer number  $N$ . The s-SNOM amplitude data  $S(\omega)$  (blue dots) at different  $N$  were normalized to  $S(\omega)$  at  $N = 6$  at  $\omega_{\text{TO}} = 1366 \text{ cm}^{-1}$ . In general, the intensity of the phonon resonance increases with  $N$  in hBN. In ultra-thin hBN crystals with  $N < 20$  [Fig. 2(b)], the intensity of the phonon resonance scales strongly with  $N$ :  $S(\omega)$  varies with even one atomic layer  $\Delta N = 1$ . As  $N$  increases, this evolution saturates at  $N \sim 80$ ; for hBN crystals with  $N > 80$ , adding more layers does not change the  $S(\omega)$  obviously.

This thickness-dependence suggests the possibility of controlling the intensity of phonon resonance by engineering layer number  $N$  in vdW materials. Intuitively, the larger the  $N$ , the more phonon oscillators and the higher the resonance intensity. The slow increase in the s-SNOM amplitude  $S(\omega)$  and the saturation at  $N \sim 80$  can be related to the aforementioned antenna effect of the s-SNOM technique. Briefly, the scanning tip in the s-SNOM can be modeled as an effective hyperboloid with length  $L$  [Fig. 2(b), inset].<sup>34</sup> This hyperboloidal antenna offers the strongest field close to the apex, followed by a considerable field below that gradually decays outside the tip apex. As  $N$  increases, while phonon resonance of the top constituent layers can be adequately detected by the s-SNOM tip, those from the bottom layers may not be sufficiently detected and, thus, contribute less to the total s-SNOM

signal  $S(\omega)$  and  $\Phi(\omega)$ . We modeled the s-SNOM amplitude  $S(\omega)$  with the tapping amplitude  $z_{\text{tip}}$  input from the experiments (see details in the [supplementary material](#)). The modeling results agree well with our experimental data with a reproduced thickness-dependence [red curves in Figs. 2(a) and 2(b)].

In addition to naturally abundant hBN, we performed s-SNOM experiments on isotopically pure  $\text{h}^{10}\text{BN}$  [Figs. 3(a) and 3(b)] and  $\text{h}^{11}\text{BN}$  [Figs. 3(c) and 3(d)], also with the thickness spanning from monolayers to bulk crystals. The s-SNOM data on  $\text{h}^{10}\text{BN}$  at  $\omega_{\text{TO}} = 1393 \text{ cm}^{-1}$  and  $\text{h}^{11}\text{BN}$  at  $\omega_{\text{TO}} = 1356 \text{ cm}^{-1}$ <sup>133,35</sup> reveal a similar scaling of the s-SNOM amplitude  $S(\omega)$  with the layer number  $N$ :  $S(\omega)$  increases evidently with the increasing  $N$  for  $N < 20$  [Figs. 3(b) and 3(d)] and this evolution saturates at  $N \sim 80$  [Figs. 3(a) and 3(c)]. The s-SNOM data on  $\text{h}^{10}\text{BN}$  and  $\text{h}^{11}\text{BN}$  both agree well with our modeling results (red curves in Fig. 3).

### III. MODELING PARAMETERS FOR THE s-SNOM DATA

Our nano-spectroscopy data agree with the lightning rod model<sup>34</sup> (see details in the [supplementary material](#)). Briefly, the s-SNOM tip was modeled as an effective hyperboloid [Inset of Fig. 2(b)] with the length  $L \sim 15 \mu\text{m}$ . s-SNOM tip radii  $a = 23, 25,$  and  $23 \text{ nm}$  were used to produce the modeling results in Figs. 2, 3(a), 3(b), 3(c), and 3(d), respectively. The tapping amplitude  $z_{\text{tip}} \sim 65 \text{ nm}$  was input from our experiments. The permittivity of naturally abundant hBN,  $\text{h}^{10}\text{BN}$ , and  $\text{h}^{11}\text{BN}$  was input from Ref. 36.

### IV. THICKNESS-SCALING OF PHONON POLARITON WAVELENGTH

After exploring the phonon resonance at transverse optical frequency  $\omega_{\text{TO}}$ , we systematically studied the scaling of phonon polariton wavelength  $\lambda_p$  with the layer number  $N$  in ultra-thin hBN ( $N < 20$ ). The experimental setup is similar to the first part of this

work, except the IR frequency  $\omega$  was tuned into the Reststrahlen band ( $\omega_{\text{TO}} < \omega < \omega_{\text{LO}}$ ). Using the aforementioned polariton imaging method, phonon polariton standing waves were recorded as oscillation fringes close to crystal edges in the s-SNOM phase  $\Phi(\omega)$  images taken on the hBN monolayer and multilayers [Figs. 4(a) and 4(b)]. Note that for ultra-thin hBN, the experiments should be conducted at frequency  $\omega$  ( $\omega = 1379 \text{ cm}^{-1}$  in this work) slightly above  $\omega_{\text{TO}}$  and s-SNOM phase  $\Phi(\omega)$  data can better visualize phonon polariton fringes.<sup>31</sup> At the fixed IR frequency  $\omega = 1379 \text{ cm}^{-1}$ , we examined multiple ultra-thin hBN crystals with  $N < 20$  and extracted their phonon polariton wavelength  $\lambda_p$  at various  $N$  in Fig. 4(c). In contrast to the scaling of the phonon resonance, phonon polariton wavelength  $\lambda_p$  scales linearly with  $N$ , as revealed in both the experimental data (blue dots) and the modeling results (red curve).<sup>31</sup> The observed linear scaling for phonon polaritons in hBN with  $N = 1-20$  is similar to that in thicker hBN ( $N > 20$ ).<sup>17</sup> The latter was attributed to the electromagnetic hyperbolicity, and our data in Fig. 4(c) suggest the same origin for phonon polariton scaling in ultra-thin hBN ( $N = 1-20$ ).

## V. CONCLUSIONS

IR nano-imaging data augmented with modeling results in Figs. 1–4 reveal the systematic scaling of phonon resonance and phonon polariton wavelength with the number of constituent layers in naturally abundant and isotopically pure hBN. The thickness-dependence of the phonon resonance persists down to  $\Delta N = 1$ , hence suggesting opportunities to precisely engineer phonon properties in vdW systems by the delicate control of layer number readily achieved via mechanical exfoliation and epitaxial growth.<sup>37</sup> The linear scaling of phonon polaritons in ultra-thin hBN shares similar features as that in relatively thick hyperbolic materials and, therefore, suggests that hBN atomic layers can be treated as thin slabs with the effective thickness of interatomic spacing (0.33 nm for hBN) and can be stacked together while still preserving electromagnetic hyperbolicity even in each atomic layer. The thickness dependence of the in-plane phonon resonance is expected to be a generic or valuable reference for investigating other fundamental resonances in vdW materials and heterostructures. Future works should be directed toward advanced vdW engineering by twisting, separating, and heterostructuring atomic layers for a more significant degree of control of phonon properties and assembling on-demand vdW devices for desired thermal and nanophotonic applications. It is also promising to study confined-induced effects on phonon resonances in delicately designed hBN nano-cavities.<sup>38,39</sup>

## SUPPLEMENTARY MATERIAL

See the [supplementary material](#) for the details of near-field results of  $\text{h}^{10}\text{BN}$  and  $\text{h}^{11}\text{BN}$ , the theoretical model, and other information.

## ACKNOWLEDGMENTS

Work at Auburn University was supported by the National Science Foundation (NSF) under Grant No. DMR-2005194, the Auburn University Intramural Grants Program, and CPU2AL seed

grant. The hBN crystal growth was supported by NSF Grant No. CMMI 1538127. W.C. acknowledges the support from the Guangdong Major Project of Basic and Applied Basic Research (No. 2020B0301030009), the National Natural Science Foundation of China (NNSFC) (Nos. 12074200 and 12004196), and 111 Project (No. B07013).

## AUTHOR DECLARATIONS

### Conflict of Interest

The authors have no conflicts to disclose.

### Author Contributions

**Xiaojie Jiang:** Data curation (lead); Formal analysis (lead); Investigation (equal); Methodology (equal); Software (equal); Validation (equal); Visualization (equal); Writing – original draft (equal); Writing – review & editing (equal). **Mingyuan Chen:** Data curation (supporting); Investigation (equal); Writing – original draft (equal); Writing – review & editing (equal). **Jiahao Li:** Data curation (supporting); Investigation (supporting); Writing – original draft (equal); Writing – review & editing (equal). **Parvin Fathi-Hafshejani:** Data curation (supporting); Formal analysis (supporting); Investigation (supporting); Software (supporting); Validation (supporting); Visualization (supporting); Writing – original draft (equal); Writing – review & editing (equal). **Jialiang Shen:** Formal analysis (supporting); Investigation (supporting); Writing – original draft (equal); Writing – review & editing (equal). **Yiming Jin:** Data curation (supporting); Formal analysis (supporting); Investigation (supporting); Methodology (equal); Software (equal); Validation (supporting); Visualization (supporting). **Wei Cai:** Funding acquisition (equal); Investigation (equal); Supervision (equal); Validation (equal); Writing – original draft (equal); Writing – review & editing (equal). **Masoud Mahjouri-Samani:** Funding acquisition (equal); Investigation (equal); Supervision (equal); Validation (equal); Visualization (equal); Writing – original draft (equal); Writing – review & editing (equal). **James Edgar:** Funding acquisition (equal); Investigation (equal); Supervision (equal); Validation (equal); Writing – original draft (equal); Writing – review & editing (equal). **Siyuan Dai:** Conceptualization (lead); Formal analysis (equal); Funding acquisition (lead); Investigation (lead); Methodology (equal); Project administration (equal); Supervision (lead); Validation (equal); Visualization (equal); Writing – original draft (equal); Writing – review & editing (equal).

## DATA AVAILABILITY

The data that support the findings of this study are available from the corresponding authors upon reasonable request.

## REFERENCES

- Y. K. Koh, in *Encyclopedia of Nanotechnology*, edited by B. Bhushan (Springer Netherlands, Dordrecht, 2012), pp. 2704–2711.
- G. Chen, *Phys. Rev. B* 57(23), 14958–14973 (1998).
- J. Sonntag, J. Li, A. Plaud, A. Loiseau, J. Barjon, J. H. Edgar, and C. Stampfer, *2D Mater.* 7(3), 031009 (2020).
- E. H. Hwang and S. Das Sarma, *Phys. Rev. B* 77(11), 115449 (2008).

- <sup>5</sup>R. Hillenbrand, T. Taubner, and F. Keilmann, *Nature* **418**(6894), 159–162 (2002).
- <sup>6</sup>A. P. Raman, M. A. Anoma, L. Zhu, E. Rephaeli, and S. Fan, *Nature* **515**(7528), 540–544 (2014).
- <sup>7</sup>S. Shen, A. Narayanaswamy, and G. Chen, *Nano Lett.* **9**(8), 2909–2913 (2009).
- <sup>8</sup>K. Y. Fong, H.-K. Li, R. Zhao, S. Yang, Y. Wang, and X. Zhang, *Nature* **576**(7786), 243–247 (2019).
- <sup>9</sup>B. Lyu, H. Li, L. Jiang, W. Shan, C. Hu, A. Deng, Z. Ying, L. Wang, Y. Zhang, H. A. Bechtel, M. C. Martin, T. Taniguchi, K. Watanabe, W. Luo, F. Wang, and Z. Shi, *Nano Lett.* **19**(3), 1982–1989 (2019).
- <sup>10</sup>J. Caldwell, L. Lindsay, V. Giannini, I. Vurgaftman, T. Reinecke, S. Maier, and O. Glembocki, *Nanophotonics* **4**, 44 (2015).
- <sup>11</sup>D. N. Basov, M. M. Fogler, and F. J. García de Abajo, *Science* **354**(6309), aag1992 (2016).
- <sup>12</sup>T. Low, A. Chaves, J. D. Caldwell, A. Kumar, N. X. Fang, P. Avouris, T. F. Heinz, F. Guinea, L. Martin-Moreno, and F. Koppens, *Nat. Mater.* **16**, 182 (2017).
- <sup>13</sup>T. Taubner, D. Korobkin, Y. Urzhumov, G. Shvets, and R. Hillenbrand, *Science* **313**(5793), 1595 (2006).
- <sup>14</sup>M. Autore, P. Li, I. Dolado, F. J. Alfaro-Mozaz, R. Esteban, A. Atxabal, F. Casanova, L. E. Hueso, P. Alonso-González, J. Aizpurua, A. Y. Nikitin, S. Vélez, and R. Hillenbrand, *Light Sci. Appl.* **7**(4), 17172 (2018).
- <sup>15</sup>J. D. Caldwell, A. V. Kretinin, Y. Chen, V. Giannini, M. M. Fogler, Y. Francescato, C. T. Ellis, J. G. Tischler, C. R. Woods, A. J. Giles, M. Hong, K. Watanabe, T. Taniguchi, S. A. Maier, and K. S. Novoselov, *Nat. Commun.* **5**, 5221 (2014).
- <sup>16</sup>Z. Shi, H. A. Bechtel, S. Berweger, Y. Sun, B. Zeng, C. Jin, H. Chang, M. C. Martin, M. B. Raschke, and F. Wang, *ACS Photonics* **2**(7), 790–796 (2015).
- <sup>17</sup>S. Dai, Z. Fei, Q. Ma, A. S. Rodin, M. Wagner, A. S. McLeod, M. K. Liu, W. Gannett, W. Regan, K. Watanabe, T. Taniguchi, M. Thiemens, G. Dominguez, A. H. C. Neto, A. Zettl, F. Keilmann, P. Jarillo-Herrero, M. M. Fogler, and D. N. Basov, *Science* **343**(6175), 1125–1129 (2014).
- <sup>18</sup>X. G. Xu, B. G. Ghamsari, J.-H. Jiang, L. Gilburd, G. O. Andreev, C. Zhi, Y. Bando, D. Golberg, P. Berini, and G. C. Walker, *Nat. Commun.* **5**, 4782 (2014).
- <sup>19</sup>S. Dai, Q. Ma, T. Andersen, A. S. McLeod, Z. Fei, M. K. Liu, M. Wagner, K. Watanabe, T. Taniguchi, M. Thiemens, F. Keilmann, P. Jarillo-Herrero, M. M. Fogler, and D. N. Basov, *Nat. Commun.* **6**, 6963 (2015).
- <sup>20</sup>S. Dai, Q. Ma, M. K. Liu, T. Andersen, Z. Fei, M. D. Goldflam, M. Wagner, K. Watanabe, T. Taniguchi, M. Thiemens, F. Keilmann, G. C. A. M. Janssen, S. E. Zhu, P. Jarillo-Herrero, M. M. Fogler, and D. N. Basov, *Nat. Nanotechnol.* **10**, 682 (2015).
- <sup>21</sup>P. Li, M. Lewin, A. V. Kretinin, J. D. Caldwell, K. S. Novoselov, T. Taniguchi, K. Watanabe, F. Gaussmann, and T. Taubner, *Nat. Commun.* **6**(1), 7507 (2015).
- <sup>22</sup>E. Yoxall, M. Schnell, A. Y. Nikitin, O. Txoperena, A. Woessner, M. B. Lundberg, F. Casanova, L. E. Hueso, F. H. L. Koppens, and R. Hillenbrand, *Nat. Photonics* **9**, 674 (2015).
- <sup>23</sup>M. Chen, S. Sanders, J. Shen, J. Li, E. Harris, and C.-C. Chen, *et al. Adv. Opt. Mater.* **10**(3), 2102723 (2022).
- <sup>24</sup>W. Ma, P. Alonso-González, S. Li, A. Y. Nikitin, J. Yuan, J. Martín-Sánchez, J. Taboada-Gutiérrez, I. Amenabar, P. Li, S. Vélez, C. Tollan, Z. Dai, Y. Zhang, S. Sriram, K. Kalantar-Zadeh, S.-T. Lee, R. Hillenbrand, and Q. Bao, *Nature* **562**(7728), 557–562 (2018).
- <sup>25</sup>Z. Zheng, N. Xu, S. L. Oscurato, M. Tamagnone, F. Sun, Y. Jiang, Y. Ke, J. Chen, W. Huang, W. L. Wilson, A. Ambrosio, S. Deng, and H. Chen, *Sci. Adv.* **5**(5), eaav8690 (2019).
- <sup>26</sup>M. Chen, X. Lin, T. H. Dinh, Z. Zheng, J. Shen, Q. Ma, H. Chen, P. Jarillo-Herrero, and S. Dai, *Nat. Mater.* **19**(12), 1307–1311 (2020).
- <sup>27</sup>J. Duan, N. Capote-Robayna, J. Taboada-Gutiérrez, G. Álvarez-Pérez, I. Prieto, J. Martín-Sánchez, A. Y. Nikitin, and P. Alonso-González, *Nano Lett.* **20**(7), 5323–5329 (2020).
- <sup>28</sup>J. Shen, Z. Zheng, T. Dinh, C. Wang, M. Chen, P. Chen, *et al. Appl. Phys. Lett.* **120**(11), 113101 (2022).
- <sup>29</sup>A. Poddubny, I. Iorsh, P. Belov, and Y. Kivshar, *Nat. Photonics* **7**, 948 (2013).
- <sup>30</sup>G. Hu, J. Shen, C.-W. Qiu, A. Alù, and S. Dai, *Adv. Opt. Mater.* **8**(5), 1901393 (2020).
- <sup>31</sup>S. Dai, W. Fang, N. Rivera, Y. Stehle, B.-Y. Jiang, J. Shen, R. Y. Tay, C. J. Ciccarino, Q. Ma, D. Rodan-Legrain, P. Jarillo-Herrero, E. H. T. Teo, M. M. Fogler, P. Narang, J. Kong, and D. N. Basov, *Adv. Mater.* **31**(37), 1806603 (2019).
- <sup>32</sup>S. Liu, R. He, L. Xue, J. Li, B. Liu, and J. H. Edgar, *Chem. Mater.* **30**(18), 6222–6225 (2018).
- <sup>33</sup>T. Q. P. Vuong, S. Liu, A. Van der Lee, R. Cuscó, L. Artús, T. Michel, P. Valvin, J. H. Edgar, G. Cassabo, and B. Gil, *Nat. Mater.* **17**(2), 152–158 (2018).
- <sup>34</sup>A. S. McLeod, P. Kelly, M. D. Goldflam, Z. Gainsforth, A. J. Westphal, G. Dominguez, M. H. Thiemens, M. M. Fogler, and D. N. Basov, *Phys. Rev. B* **90**(8), 085136 (2014).
- <sup>35</sup>R. Cuscó, J. Edgar, S. Liu, G. Cassabo, B. Gil, and L. Artús, *J. Phys. D: Appl. Phys.* **52**(30), 303001 (2019).
- <sup>36</sup>A. J. Giles, S. Dai, I. Vurgaftman, T. Hoffman, S. Liu, L. Lindsay, C. T. Ellis, N. Assefa, I. Chatzakis, T. L. Reinecke, J. G. Tischler, M. M. Fogler, J. H. Edgar, D. N. Basov, and J. D. Caldwell, *Nat. Mater.* **17**, 134 (2018).
- <sup>37</sup>M. I. Bakti Utama, Q. Zhang, J. Zhang, Y. Yuan, F. J. Belarar, J. Arbiol, and Q. Xiong, *Nanoscale* **5**(9), 3570–3588 (2013).
- <sup>38</sup>Z. Sun, Á. Gutiérrez-Rubio, D. N. Basov, and M. M. Fogler, *Nano Lett.* **15**(7), 4455–4460 (2015).
- <sup>39</sup>A. J. Giles, S. Dai, O. J. Glembocki, A. V. Kretinin, Z. Sun, C. T. Ellis, J. G. Tischler, T. Taniguchi, K. Watanabe, M. M. Fogler, K. S. Novoselov, D. N. Basov, and J. D. Caldwell, *Nano Lett.* **16**(6), 3858–3865 (2016).